

Deviations From Axisymmetry Revealed by Line Polarization in the Normal Type Ia SN 2004S

Ryan Chornock & Alexei V. Filippenko

Department of Astronomy, University of California, Berkeley, CA 94720-3411

chornock@astro.berkeley.edu

ABSTRACT

We present a single epoch of high signal-to-noise ratio spectropolarimetry of the Type Ia supernova (SN Ia) 2004S taken nine days after maximum light. The flux spectrum is normal, but with the additional presence of high-velocity (HV) line features in both Ca II and Fe II. The object shows continuum polarization at the 0.4% level in the red, a value which appears to be typical of SNe Ia. The continuum data are consistent with a \sim 10% global asphericity in an axisymmetric geometry. Unlike previous observations of other SNe Ia with HV features, the HV features in SN 2004S show no strong polarimetric signature, though this may be due to the timing of our observations. Instead, the object shows line polarization features ($P \leq 0.5\%$) that are rotated with respect to the axis of symmetry of the continuum. The line features are visible in Si II, Fe II, and Ca II, and appear to be narrowly confined in velocity space just above the photosphere. These polarization features are a result of compositional inhomogeneities in the ejecta. They may represent newly synthesized elements whose clumpy spatial distribution within the ejecta is distinct from that of the globally aspherical ejecta as a whole.

Subject headings: supernovae: individual (SN 2004S) — polarization

1. Introduction

Carbon-oxygen white dwarfs that accrete enough mass to approach the Chandrasekhar limit can explode as Type Ia supernovae (SNe Ia). The first successful models of the explosion process invoked parameterized one-dimensional (1D) flame fronts propagating outward from the center of the star as a subsonic deflagration (Nomoto et al. 1984). However, the explosion process is fundamentally three-dimensional (3D) in nature as the propagation of a

deflagration front is marked by large-scale fluid motions and mixing due to Rayleigh-Taylor instabilities. Recent 3D pure deflagration models are not as successful at reproducing the observations because the simulated explosions are underluminous, underenergetic, inefficient in burning the available fuel, and result in ejecta that are too well-mixed (Reinecke et al. 2002; Gamezo et al. 2003; Kozma et al. 2005).

Some modelers interpret these results as requiring the burning front to make a transition from a subsonic deflagration to a supersonic detonation as it becomes turbulent (Khokhlov 1991), though the details of how this might happen are unclear (Hillebrandt & Niemeyer 2000). Simulations, such as those of Gamezo et al. (2005), demonstrate that models with different prescriptions for the evolution of the burning front produce quite different ejecta structures. Observational probes of the geometry and structure of the ejecta are therefore necessary in light of the lack of an *a priori* theoretical understanding of the explosion.

The deviations from spherical symmetry seen in the simulations discussed above are a result of the ignition process and the random physics of turbulent flame propagation. More systematic departures from sphericity could be a signature of the progenitor systems, which are largely unknown (Branch et al. 1995; Livio 2001; Nomoto et al. 2003), or their environments. Rotational flattening of the progenitor white dwarf, interaction with circumstellar material, or the process of merging two white dwarfs could lead to SNe Ia with large-scale asphericities (Howell et al. 2001; Wang et al. 2003).

Spectropolarimetry provides a unique opportunity to probe the geometry of SNe Ia. Outward streaming radiation in a supernova atmosphere acquires a polarization when it is scattered by electrons. Distant supernovae are unresolved by the observer, so the net polarization of the received light represents an integration of emitted flux over the visible surface of the object. In the case of a spherical supernova, symmetry demands that the total polarization be zero. Non-zero net polarization is therefore a sign of some deviation from spherical symmetry in the system (Shapiro & Sutherland 1982).

Global asphericities of the photosphere, such as ellipsoidal deformations, are manifested as net continuum polarization (Jeffery 1991; Höflich 1991). Past investigations of SNe Ia have found typical intrinsic polarizations of order a few tenths of a percent in the continuum. The object with the highest measured intrinsic continuum polarization percentage is still the subluminous SN 1999by (Howell et al. 2001), which showed at least 0.7% polarization. Howell et al. (2001) found that the spectropolarimetric data could be modeled by an oblate spheroid with an axial length ratio of 1.17, seen nearly equator-on. The lower continuum polarizations measured in the half-dozen other SNe Ia with good data are consistent with global asphericities at the $\sim 10\%$ level (Wang et al. 2003, 2006; Leonard et al. 2005; Chornock et al. 2006).

Line polarization allows other approaches to the study of asphericity. Polarization modulations and angle rotations across a spectral feature could be a sign of an aspherical distribution of that ionic species. Leonard et al. (2005) found that the angle rotations seen in spectral features of some SNe Ia could be due to clumps or ionization asymmetries in the ejecta. Even if the ejecta lack such compositional inhomogeneities, line polarization can give insight into the global asphericity of the ejecta. Photons scattered in a line are generally depolarized (Höflich et al. 1996), but in a purely ellipsoidal geometry we should expect strong, isolated lines to be associated with “inverted” P-Cygni polarization line profiles (Jeffery 1989). The effect of many overlapping lines is to produce a decrease in the polarization at the same angle as the continuum, as was seen in SN 1999by (Howell et al. 2001). These signatures of asphericity are largely independent of the uncertainties in the removal of interstellar polarization (ISP) that plague estimates of the continuum polarization.

One exciting recent development in SN Ia research is the association of “high-velocity” (HV) features in the flux spectra with strong spectropolarimetric features. These HV features are so-named because they are signatures of a separate line-formation region at higher velocities than the normal photospheric component. Separate HV material was first noticed in the Fe II lines of SN 1994D by Hatano et al. (1999), but it may be ubiquitous in SNe Ia. Every object in the sample of Mazzali et al. (2005b) showed evidence of HV absorption in the Ca II near-infrared (NIR) triplet if the spectra were taken at sufficiently early epochs.

The HV Ca II NIR triplet feature in the otherwise-normal SN 2001el was responsible for a 0.7% spectropolarimetric feature that was rotated with respect to the continuum (Wang et al. 2003; Kasen et al. 2003). This feature was modeled as forming in a spatially separate region that did not share an axis of symmetry with the continuum (Kasen et al. 2003). Subsequent observations of the SNe Ia 2004dt and 2002bf (Leonard et al. 2005; Wang et al. 2006) also showed strong polarization modulations across the HV lines. The composition and origin of this HV material remain mysterious. Suggestions in the literature have included clumps of material newly synthesized in the explosion (Wang et al. 2003), signatures of a gravitationally confined detonation (Kasen & Plewa 2005), and interaction with circumstellar material (Wang et al. 2003; Gerardy et al. 2004; Mazzali et al. 2005a). In all cases, viable models for the origin of the HV material must recognize its intrinsically 3D nature, as revealed by the spectropolarimetric line features and angle rotations.

Inverting the observed polarization data for one object to construct a model is highly underconstrained. A more fruitful approach is to collect data for a sample of objects to see which, if any, model can best match the range of observed polarimetric behaviors. Though observations are still sparse, Leonard et al. (2005) have shown that SNe Ia exhibit diverse polarimetric characteristics that may correlate with other photometric and spectroscopic

properties. For example, the two SNe Ia with the highest observed intrinsic continuum polarizations are both subluminous, and the objects with HV features have shown the largest line polarizations. In addition, Wang, Baade, & Patat (2007) have claimed to find a correlation between the strength of the spectropolarimetric modulation across the Si II $\lambda 6355$ feature and the light-curve shape (a luminosity indicator) for a sample of SNe Ia.

In this paper we add to the small sample of SNe Ia observed spectropolarimetrically and present a single epoch of high signal-to-noise-ratio (S/N) observations of SN 2004S, a SN Ia with HV features that is a virtual twin of SN 2001el. The data were taken 9 d after maximum light and the observed continuum polarization provides evidence for asphericity in the ejecta. Deviations from axisymmetry, seen as spectropolarimetric modulations across prominent spectral lines, are the main result and focus of the discussion below.

2. Observations

SN 2004S in MCG –05–16–021 was discovered by R. Martin on 2004 February 3.542 (UT dates are used throughout this paper; Martin & Briggs 2004) and spectroscopically identified as a SN Ia by Suntzeff et al. (2004). Optical photometry of SN 2004S has been published by both Misra et al. (2005) and Krisciunas et al. (2007), with the latter authors adding a significant near-IR light curve. They both find SN 2004S to be photometrically normal and we adopt a date for *B*-band maximum light of February 4.37 ± 0.25 (Krisciunas et al. 2007). Krisciunas et al. (2007) emphasize that SN 2004S and SN 2001el were found to be photometric twins. In addition, the spectra were very similar, with both objects showing a strong HV component to the Ca II NIR triplet lines at early times.

We observed SN 2004S on 2004 February 13.34 (+9 d after maximum light) for a total of 3600 s using the polarimeter unit¹ of the Low Resolution Imaging Spectrometer (LRIS; Oke et al. 1995) on the Keck I 10-m telescope. The D560 dichroic beamsplitter sent blue light to a 400/3400 grism and transmitted red light to the 400/8500 grating. The 1.5''-wide slit gave a spectral resolution of about 9 Å over the full observed wavelength range of 3040–9250 Å. The slit was aligned at 180°, which was near the parallactic angle for the first observation. Conditions were good and the seeing was $\sim 0.9''$ during these observations.

Standard two-dimensional (2D) image-processing tasks were performed using the pack-

¹See http://alamoana.keck.hawaii.edu/inst/lris/polarimeter/manual/pol_v3.ps for the online polarimeter manual by M. Cohen (2005).

ages in IRAF², as were the optimal extraction of spectra and wavelength calibration. We used our own routines for flux calibration and atmospheric absorption correction of the 1D spectra (Matheson et al. 2000). The high airmass (~ 1.6) and fixed position angle of the slit combined to make the effects of atmospheric dispersion (Filippenko 1982) apparent in our data. As the first observation was taken close to the parallactic angle, we adjusted the continuum slope of the combined flux spectrum to that of the first observation by dividing the total spectrum by a low-order spline fit to the ratio of the two spectra.

The spectropolarimetric reductions followed the standard procedure outlined by Miller et al. (1988) and implemented by Leonard et al. (2001). The zero point of the waveplate was determined by setting the observed position angle of the polarization standard star BD +59 389 to the catalogued value of 98.09° (Schmidt et al. 1992). As a check on the polarization angle, we also observed a lower-quality polarization standard, HD 127769. The literature measurements for the polarization vary somewhat, and the published angles are 54.0° and 52.7° (Clemens & Tapia 1990; Mathewson & Ford 1970). We measured an angle of 52.5° , which allows us to conclude that our observation of BD +59 389 gave a reliable zero point. Two null polarization standards, HD 109055 and HD 57702 (Berdyugin et al. 1995; Clemens & Tapia 1990; Mathewson & Ford 1970), were also observed and had negligible polarization ($P < 0.07\%$).

Dichroic absorption by interstellar dust along the line of sight polarizes light from the supernova. We selected two stars, CD –31 3659 and HD 48649, to act as probes of the Galactic contribution to the total ISP and observed them immediately after the supernova. Both are A-type stars more than 150 pc above the Galactic plane and within 0.6° of SN 2004S; they can be regarded as intrinsically unpolarized probes that are distant enough to sample almost all of the dust along that line of sight out of our Galaxy, following the suggestion of Tran (1995).

The same dust that polarizes also reddens the light, which allows us to anticipate the magnitude of the effect of ISP. The Galactic extinction along the line of sight has $E(B-V) = 0.101$ mag (Schlegel et al. 1998). Empirically, dust in our Galaxy shows a polarization efficiency ($P_{MAX} / E(B-V)$) of typically $3\% \text{ mag}^{-1}$, with a maximum value of $9\% \text{ mag}^{-1}$ (Serkowski et al. 1975), so we should expect the polarization to be $\sim 0.3\%$ if the line of sight is typical, up to a maximum of 0.9% . We integrated the flux-weighted Stokes parameters over 5050–5950 Å to approximate the V -band polarization ($q_{V,uv}$) and

²IRAF is distributed by the National Optical Astronomy Observatories (NOAO), which is operated by the Association of Universities for Research in Astronomy, Inc., under cooperative agreement with the National Science Foundation.

measured (0.03, 0.49) and (0.11, 0.30), respectively, for the two probe stars. The two stars have somewhat different polarization, so we averaged their Stokes parameters to form our estimate of the Galactic ISP. Smoothed versions of q and u were then subtracted from the SN 2004S observations. Uncertainties in the determination of the Galactic ISP are absorbed into the determination of the host-galaxy contribution to ISP below.

3. Results

3.1. Total-Flux Spectrum

The high S/N total-flux spectrum is presented in Figure 1 along with a spectrum of the prototypical normal Type Ia SN 1989B (Wells et al. 1994). We have removed a radial velocity for the host galaxy of SN 2004S of $2808 \pm 5 \text{ km s}^{-1}$ (determined from 21-cm observations by Theureau et al. (2005)) from all plots in this paper. The SN 1989B spectrum is from 8 d after B -band maximum light and is very similar to our SN 2004S spectrum, confirming that the age inferred from the photometry is accurate. Wells et al. (1994) measured the photometric decline-rate parameter (Phillips 1993) for SN 1989B to be $\Delta m_{15}(B) = 1.31 \pm 0.07 \text{ mag}$, compared to the value of $1.14 \pm 0.01 \text{ mag}$ reported by Krisciunas et al. (2007) for SN 2004S.

We shall use the fiducial SN 1989B spectrum as a reference to better understand SN 2004S. The most obvious difference between the two spectra is that the absorptions due to Ca II are significantly deeper in SN 2004S and extend to much higher velocities. SN 2004S otherwise appears to be spectroscopically quite normal for a SN Ia (Filippenko 1997). A more complete spectroscopic sequence is presented in Krisciunas et al. (2007), along with comparisons to a suite of SNe Ia.

Figure 2 shows a closer view of the spectral features due to Ca II and Si II. The Si II $\lambda 6355$ line in particular is the hallmark of SNe Ia and is frequently used to measure the photospheric velocity (e.g., Branch et al. 1988). As shown in the middle panel of Figure 2, the absorption minimum of the Si II line in SN 1989B is at $\sim 10,000 \text{ km s}^{-1}$, a typical value for a SN Ia. The Si II feature in SN 2004S is noticeably weaker and the minimum is at only 8900 km s^{-1} , compared to the figure of 9300 km s^{-1} reported by Suntzeff et al. (2004) near B -band maximum light. This velocity is actually quite low for a normal SN Ia at this epoch and is comparable to the lowest-velocity objects in the sample of Benetti et al. (2005). Only peculiar subluminous objects such as SNe 1991bg and 2002cx have shown lower Si II velocities at a similar age (Leibundgut et al. 1993; Li et al. 2003).

By contrast, Figure 2 shows that the Ca II spectral features in SN 2004S were formed at higher velocities than in SN 1989B. The Ca II H&K $\lambda\lambda 3934, 3968$ absorption feature in

SN 1989B has a minimum at 3795 Å (11,600 km s^{−1}) and a rather flat-bottomed absorption with the blue wing rising to a flux maximum at 3675 Å (21,200 km s^{−1}), where the velocities reported here are relative to the *gf*-weighted line wavelength of 3945 Å. In SN 2004S, the absorption is much deeper and the flux minimum is much bluer, at 3710 Å (18,400 km s^{−1}), with absorption extending outward to 3600 Å (27,400 km s^{−1}).

The profile of the Ca II NIR triplet shown in Figure 2 is more complicated than the other two lines, with at least three distinct flux minima present near 8080, 8230, and 8385 Å. Two effects contribute to the complexity of this line profile. The first is that the feature is intrinsically formed by a triplet and the wavelength separation of the components is relatively large. The minima at 8385 and 8230 Å can then be identified with Ca II $\lambda 8662$ and $\lambda\lambda 8498, 8542$, respectively, with a blueshift of 10,000–11,000 km s^{−1}. Absorption minima at similar velocities can be seen in the reference spectrum of SN 1989B. SN 2004S shows an additional flux minimum near 18,000 km s^{−1} with no corresponding feature in SN 1989B, which we identify as the counterpart of the high-velocity absorption seen in Ca II H&K. There are therefore two Ca II line-forming regions in SN 2004S, one at the photosphere and a second one separated from the photosphere by 8,000 km s^{−1}. No photospheric component is visible in the H&K feature, which is dominated by the HV component. The spectral sequence of SN 2004S presented by Krisciunas et al. (2007) shows the evolution of the Ca II NIR triplet absorption profile from being dominated by HV material at early times to photospheric velocities at late times.

The exact velocity range of this HV absorption is difficult to determine directly from the spectrum because of confusion caused by line blending. If the minimum at 8080 Å is identified with $\lambda 8542$, then the apparent velocity is 16,700 km s^{−1}, but at that velocity the $\lambda 8662$ line would produce an absorption at 8190 Å, which is close to a local maximum in the line profile. It is likely that the HV material is at slightly higher velocity (such as 18,000 km s^{−1}), but with a velocity spread sufficient to blend the two components of the line profile together. A spectral synthesis calculation is necessary to make a more quantitative estimate of the velocity spread of the HV material. The maximum velocity of the absorbing material is easier to isolate, as the blue edge of the feature is at 7880 Å (24,000 km s^{−1} if identified with $\lambda 8542$).

As with all supernova spectral features, blends with other lines due to the large Doppler shifts may affect the strength and apparent wavelength of any given spectral feature. In particular, Si II $\lambda 3858$ and O I $\lambda 8446$ are candidates for making a potential contribution to the H&K and NIR triplet features, respectively. We do feel confident in identifying the presence of a high-velocity absorption component in Ca II, especially with the simultaneous detection of a feature at a similar velocity in both the H&K and NIR triplet features. We

note that no HV component is obvious in the profile of the Si II $\lambda 6355$ line. There are notches in the blue wing, but these are the early signs of incipient iron lines that strengthen with time, not HV features (see the spectral sequence in Krisciunas et al. 2007).

3.2. Spectropolarimetry

The last step of preparation before we can begin analysis of the spectropolarimetry is to correct the data for ISP in the host galaxy. Normal SNe Ia have well-defined colors as a function of age, so Misra et al. (2005) were able to estimate a total $E(B-V)$ to SN 2004S of 0.18 ± 0.05 mag by comparison with templates. The numbers given above imply that the host galaxy contributes $E(B-V) \approx 0.08$ mag of reddening, so we expect a typical host ISP of $\sim 0.24\%$ (Serkowski et al. 1975). Krisciunas et al. (2007) used the long baseline of their optical through NIR observations to set a tighter constraint on the extinction. They derive a host extinction of $A_V = 0.071 \pm 0.043$ mag, which would imply a host ISP of 0.07% for typical dust, up to a maximum of 0.21%. Unlike the Galactic ISP, we have no method to directly measure the host contribution, so we will have to appeal to some interpretation of the SN polarimetry itself to make an ISP estimate. This ISP estimate will not be unique because different assumptions about the intrinsic SN polarization can lead to different ISP estimates.

Some of the SN 2004S spectropolarimetry data are plotted in the Stokes $q - u$ plane in Figure 3. Each circle represents a wavelength bin 50 Å wide and the size of each is proportional to the wavelength of the bin it represents, so larger circles are from longer wavelengths. Anticipating the results below, we only plot data points from sections of the spectrum that we believe are free from strong line polarization features. The exact wavelength choices for these “continuum” data points are marked in the middle panel of Figure 4. The wavelength dependence of ISP is sufficiently weak at optical wavelengths (Serkowski et al. 1975) that the effect of subtracting a small ISP is similar to choosing a new origin for the data in the $q - u$ plane. The distribution of plotted wavelength bins is elongated, with a clear spread of at least 0.4% in polarization between the blue end of the spectrum (smaller points) and the red end (larger points), which must be due to intrinsic SN polarization. The dotted circle in Figure 3 has a radius of 0.21%, corresponding to the maximum expected host ISP.

The line plotted in Figure 3 is a fit to the data points. The simplest decomposition of the polarization is to choose an ISP vector that lies on the line and to assign the remaining polarization to intrinsic SN polarization that varies in amplitude as a function of wavelength, with most of the variation occurring along the axis defined by the line. The

direction indicated by the line could then represent the symmetry axis of the SN continuum as projected onto the sky (Wang et al. 2001). This argument does not give a unique value for the ISP, so we will appeal to SN Ia theory and spectral modeling calculations to assume that the intrinsic polarization at blue wavelengths must be small. As Howell et al. (2001) have argued, many overlapping lines of iron-peak elements are the dominant form of opacity in SNe Ia at wavelengths below 6000 Å. The opacity from these lines should destroy any polarization caused by electron scattering in an aspherical SN atmosphere. Howell et al. (2001) then chose an ISP vector to make the polarization zero at the blue end of their data. Other authors (Leonard et al. 2005; Wang et al. 2006; Chornock et al. 2006) have chosen ISP vectors to make the intrinsic polarization of certain blue emission features zero.

For this work, we will select an ISP vector (q_{ISP}, u_{ISP}) that lies on the line in Figure 3. The exact point along this line is arbitrary, but we chose the point $(-0.040, -0.159)$, which we have marked with a square, in order to make the polarization small at blue wavelengths. A host ISP of this magnitude is consistent with the reddening constraints mentioned above. We subtracted an ISP with the wavelength dependence of Serkowski et al. (1975) and assumed $R_V = A_V/E(B - V) = 3.1$.

The formal polarization [$P = (q^2 + u^2)^{\frac{1}{2}}$] is positive-definite and is therefore biased high for low values of the polarization. We can avoid this bias by continuing to represent the data by two Stokes parameters, but we are free to choose a more convenient parameterization of rotated Stokes parameters (RSP; Trammell et al. 1993). In this case, we will rotate the ISP-subtracted data to align one Stokes parameter (called q_{RSP}) with the obvious axis seen in the continuum data in Figure 3 and marked by the line. This coordinate system is similar to the decomposition of polarization into a dominant and orthogonal axis by Wang et al. (2003), except that we have explicitly excluded wavelengths of strong line polarization from the fit.

The rotated SN 2004S spectropolarimetry is plotted in Figure 4. After the rotation, most of the continuum polarization is in the q_{RSP} Stokes parameter. The polarization rises from near zero at 4000 Å to a maximum of 0.4% at 6800 Å before declining at longer wavelengths. Several broad undulations in the continuum polarization are apparent as well as narrower features associated with spectral lines seen in the flux spectrum. Five of these narrower features are also visible as strong negative departures from the continuum in the u_{RSP} parameter and hence as rotations in θ . Spectral windows away from these narrower features are mostly flat and near zero in u_{RSP} despite the broad undulations in q_{RSP} , justifying our decomposition of the polarization into these Stokes parameters. We now consider the line features in more detail.

3.2.1. Silicon

We will first examine the polarization of the Si II $\lambda 6355$ line because it is the most isolated and can be used as a reference to understand the other spectropolarimetric features. As noted above, the continuum polarization of SN 2004S is confined to q_{RSP} , while Figure 4 shows that the Si II line has excursions away from the continuum polarization in both q_{RSP} and u_{RSP} . We can immediately conclude that the Si II line-formation region does not share an axis of symmetry with the continuum.

This point is reinforced in the upper-left panel of Figure 5, where data points from both the continuum and the line are plotted in the $q - u$ plane. The continuum points are the same as in Figure 3, but rotated into the new coordinate system and shown in gray. The elongation of the continuum points along a line in the $q - u$ plane was argued above to be representative of scattering in a geometry with a single well-defined axis. The data points in black with error bars are 50 Å bins between wavelengths of 5900 and 6400 Å. These line polarization points clearly do not share the same distribution in the $q - u$ plane as the continuum. They are arranged along a linear axis that is rotated with respect to, and intersects the major axis of, the spread of continuum points.

Another view of the same data can be seen in the leftmost panels of Figure 6, where the Stokes parameters are plotted as a function of velocity in the line in 20 Å bins. The Si II $\lambda 6355$ line is located in the middle of a broad depression in q_{RSP} , which has local maxima near 5700 and 6800 Å. There is a narrower, sharp feature in q_{RSP} located just blueward of the minimum of the line in the flux spectrum. This feature is at a similar velocity as the largest negative depression in u_{RSP} . The flux minimum of the line is at 8900 km s⁻¹ and the greatest deviation of the line polarization from the continuum is in the narrow range of approximately 9,000-11,000 km s⁻¹, just above the photosphere.

Interestingly, as one moves to redder wavelengths from the flux minimum of the $\lambda 6355$ line, u_{RSP} increases from its minimum, crosses zero near 6350 Å (~ 0 km s⁻¹), and rises to a peak in the red wing of the emission component of the line. This positive excursion in u_{RSP} returns to zero (the continuum value) near 6700 Å, corresponding to a redshift of $\sim 16,000$ km s⁻¹, which may be a spectropolarimetric indication of Si II forming in the far side of the ejecta almost as far out as the expansion velocity derived above for the HV line-formation region.

3.2.2. Calcium

The next ionic species we examine is Ca II. The analysis of the flux spectrum above presented evidence for two Ca II line-formation regions, at 10,000 and 18,000 km s^{−1}, making the shape of the NIR triplet in the flux spectrum complicated. The polarization profile of the NIR triplet shown in Figure 4 is also complex. Two separate polarization features are seen in both q_{RSP} and u_{RSP} near 8165 and 8345 Å.

The presence of two line-formation regions makes interpretation of the polarimetric features ambiguous, but the rightmost panels of Figure 6 can clarify the situation. The three lines labeled “HV” in the top right panel mark the expected location of features associated with the three components of the triplet, blueshifted by the 18,000 km s^{−1} velocity of the HV line-formation region seen in the total-flux spectrum. The stronger of the two polarimetric features is at the same velocity as the expected $\lambda 8662$ line, but no feature is seen at the expected position of the other two lines. A much more natural identification of the lines can be seen in the lower-right panel. The lines labeled “PV” mark the expected location of features associated with the NIR triplet if they occur at the same velocity (10,000 km s^{−1}) as the strongest polarization feature in the Si II line. The redder of the two polarization features is formed over a velocity range of 9,500–12,500 km s^{−1} if it is identified as Ca II $\lambda 8662$. The bluer of the two features is then a blend of $\lambda 8498$ and $\lambda 8542$ forming at similar velocities. In this interpretation, the two polarimetric features are formed at velocities just above the local minima in the total-flux spectrum ($\sim 11,000$ km s^{−1}), similar to the behavior of the Si II $\lambda 6355$ line discussed in the previous section.

The data points plotted in the $q - u$ plane in the lower-left panel of Figure 5 are 50 Å bins between 8050 and 8300 Å and correspond to the polarization feature we associated with $\lambda\lambda 8498, 8542$. Data points from the $\lambda 8662$ feature, spanning 8300 to 8500 Å, are plotted in the lower-right panel. In each panel the data points are connected in order of wavelength by a line. The location of these two features in the $q - u$ plane reveals complex spectropolarimetric behavior. Not only do these Ca II $\lambda\lambda 8498, 8542$ data points show a spread of 0.4% in each Stokes parameter, which is itself indicative of deviations from simple axisymmetry, but the line connecting the data points shows that the path in the $q - u$ plane is ordered in the form of a loop. This is in contrast with the Si II data, which form a linear feature. The $\lambda 8662$ feature shows a similar 2D spread with a suggestion of a loop, though with lower statistical significance.

3.2.3. Iron

Next we will consider the two features visible in Figure 4 as deviations from the continuum in both u_{RSP} and θ near 4800 Å. The spectra of SNe Ia in this wavelength region are formed by a complicated blend of lines (mostly Fe II, S II, and Si II), so the identity of any given spectral feature is ambiguous. The wavelengths of the strongest rotations in these features are at about 4745 and 4832 Å. We first assume that the spectropolarimetric features are formed in a similar manner to the Si II line analyzed above. The narrow core of the polarization feature in the Si II line was centered at an expansion velocity of \sim 10,000 km s $^{-1}$. De-blueshifting the unknown features by this velocity implies rest wavelengths of 4906 and 4996 Å for our mystery lines. The Ca II NIR triplet polarization feature was formed at a velocity of 11,000 km s $^{-1}$, which would imply rest wavelengths of 4922 and 5013 Å for these lines.

One reasonable identification is with Fe II $\lambda\lambda$ 4924, 5018 if those lines are blueshifted by \sim 11,000 km s $^{-1}$. There are two major complications for this interpretation. The first is that those Fe II lines form a triplet with λ 5169. All three lines share the same lower atomic level, so they should all be present if one of them is. With this identification, the stronger spectropolarimetric feature is associated with λ 4924, the weaker one with λ 5018, and λ 5169 lacks a counterpart. This ordering by strength of spectropolarimetric features is the reverse of the ordering by weighted oscillator strengths (gf). Naively, one might expect the strongest line to produce the strongest polarimetric feature, much as the strongest of the three lines produces the strongest feature in the flux spectrum.

The second complication can be seen in the flux spectrum in Figure 1. A series of flux minima at 4698, 4772, and 4885 Å are labeled as Fe II. If this identification is correct, the three components of the triplet are blueshifted by 14,000, 15,000, and 17,000 km s $^{-1}$, respectively. These velocities are much greater than the photospheric velocity measured from the Si II line, similar to the HV Ca II features discussed above, and thus raise the specter of multiple Fe II line-forming regions, one at photospheric velocity and one at high velocity. HV Fe II was first invoked by Hatano et al. (1999) to model the early-time spectra of SN 1994D and has since been used by several authors to explain spectra of SNe Ia before and near maximum light (e.g., Stehle et al. 2005). Branch et al. (2006) found that their spectral fits to a number of SNe Ia were improved with the addition of HV Fe II. Suggestively, they also found that the object in their sample whose fit required the highest optical depth in HV Fe II was SN 2001el, which also had strong HV Ca II absorption. Spectral fits that lack HV Fe II have difficulty producing alternative identifications for these absorption minima in SNe Ia.

These difficulties with the Fe II interpretation lead to the natural question of whether any other ionic species could be responsible. The first alternative identifications we consider

are Si II and Ca II because these species are known to produce polarized spectral features at other wavelengths in this object. Ca II has no strong spectral features in this wavelength region, but the Si II $\lambda 5051$ blend is a plausible candidate for creating a spectropolarimetric feature. Wang et al. (2006) identified a feature from this line in SN 2004dt, but in SN 2004S this single line would have to explain two polarimetric features. These features would be at expansion velocities of 18,700 and 13,300 km s⁻¹, significantly different from the polarimetric behavior of the strong Si II line ($\lambda 6355$), so we reject the Si II interpretation.

The most plausible remaining candidate ion is S II, which has a large number of transitions in the optical. Blends of these lines, particularly between 4500 and 5700 Å, make a contribution to the spectra of SNe Ia. The strongest spectroscopic feature in the flux spectrum attributed to S II in SNe Ia is the “W”-shaped absorption near 5300 Å (see Figure 1). No strong spectropolarimetric feature is visible in Figure 4 near this wavelength. An identification of the polarimetric features with S II would have to explain why the weaker lines leave a polarimetric signature and the stronger ones do not.

We will adopt the identification of these lines with Fe II for the rest of the paper, noting the caveats above. Data points from these two lines (50 Å bins between 4650 and 5000 Å) are plotted in the upper-right panel of Figure 5. The distribution of points in the $q - u$ plane is elongated in a linear manner along a direction roughly parallel to the linear feature seen in Si II, possibly indicating a common origin for the spectropolarimetric features. The middle panels of Figure 6 show the same data in velocity space. The expected locations of the three members of the triplet if they were present at the 15,000 km s⁻¹ velocity inferred from the flux spectrum are marked in the q_{RSP} panel, while the u_{RSP} panel shows the expected position of features at 10,000 km s⁻¹ as measured from the Si II polarization feature. The polarimetric line features do not fall at the same position as the HV notches in the flux spectrum, but they do correspond to the positions of two of the three lines at photospheric velocities.

One possible explanation for the lack of a polarimetric counterpart to $\lambda 5169$ is to rely on the observed narrowness of the sharp spectropolarimetric feature seen in the core of the Si II line and at the photospheric velocity in the Ca II NIR triplet. Perhaps whatever non-axisymmetric asphericity (e.g., clumping) is the cause of the spectropolarimetric line features and rotations in the other species is narrowly confined in the ejecta. Stronger lines are optically thick through more of the ejecta, possibly including the less dense spaces between clumps. If the $\lambda 5169$ line (with the largest gf -value) is optically thick over more of the ejecta than the other Fe II lines, then the signature of the asphericity could be hidden. Another possibility is that blending with another line (Si II $\lambda 5051$ at photospheric velocities is a possible candidate) destroys the polarization signature.

3.2.4. Non-detections

It is also worth considering which line features do not show spectropolarimetric features, as well as those that do. The S/N of our observations degrades rapidly blueward of 4000 Å due to declining efficiency of the spectrograph and increasing atmospheric absorption. Despite these mitigating effects, we are confident that Figure 4 shows no sign of strong spectropolarimetric features associated with the Ca II H&K lines of the sort seen in the NIR triplet lines of the same species. One potential explanation is that, if our choice of ISP is correct, the continuum at such short wavelengths has negligible polarization due to the high opacity in lines from iron-peak elements. The additional opacity of the strong H&K lines then results in little additional depolarization.

Two of the more interesting ionic species that lack strong polarimetric signatures are O I and S II. Oxygen in the ejecta of SNe Ia could either be unprocessed material from the progenitor white dwarf or the result of incomplete carbon burning. In either case the oxygen should not share the same spatial distribution as the silicon. SN 2004dt (Leonard et al. 2005; Wang et al. 2006) showed the combination of strong polarization in the HV Si II line features and a lack of a feature at the O I line, which Wang et al. (2006) interpreted to be a result of turbulent burning processes leaving clumpy intrusions of silicon in an oxygen-dominated substrate. The O I $\lambda 7773$ line in SN 2004S is of normal strength (see Figure 1), with a flux minimum near a radial velocity of 9,000 km s⁻¹. No strong polarization feature is visible in Figure 4 in u_{RSP} , and there is marginal evidence for an increase in q_{RSP} . Unfortunately, this line falls near the strongest atmospheric absorption at optical wavelengths (the A band) and so the S/N is somewhat degraded.

Sulfur, however, should have a spatial distribution similar to that of silicon, as both elements are formed by similar burning processes. S II is responsible for the characteristic “W”-shaped feature near 5300 Å in SNe Ia before maximum light, as well as more minor features just blueward of that. At this late epoch, the “W”-shaped feature has started to fade and the redder absorption is being dominated by the increased effect of iron on the spectrum at these wavelengths. We see no strong modulation in q_{RSP} at the position of the S II features and u_{RSP} definitely lacks the strong feature seen in the Si II line. Differences in polarization behavior between the two species despite similar spatial distributions could be a result of different optical depths in the lines, or the underlying continuum polarization could be modified differently by the blends of lines from iron-peak elements.

4. Discussion

The most basic question to be answered by spectropolarimetry is whether or not an object is spherically symmetric. The strong wavelength dependence of the polarimetric data shown above is convincing evidence of intrinsic polarization and hence of deviations from spherical symmetry in the ejecta of SN 2004S.

With the set of Stokes parameters that we have chosen to present the data, q_{RSP} would be an estimator of the total polarization if the system had a well-defined symmetry axis. The need for a second variable to describe the data, here the Stokes parameter u_{RSP} , is indicative of deviations from axisymmetry. The second parameter is significantly non-zero only for wavelength regions near certain spectral features. Equivalently, the scatter of the continuum data points about the best-fit line in Figure 3 is similar to that expected from the errors. This means the SN ejecta can be approximated as having a global, axisymmetric asphericity with deviations caused by a non-axisymmetric distribution of certain ionic species.

Polarization in a SN atmosphere is induced by light scattering off of electrons. Thomson scattering is a wavelength-independent process, but our estimator of the total polarization, q_{RSP} , shows a number of broad undulations with wavelength and a general decrease in the polarization level toward the blue end of the spectrum. This is due to the nature of the opacity in SNe Ia, which is dominated by a large number of bound-bound transitions, primarily of iron-peak elements (Pinto & Eastman 2000). These transitions act to depolarize the emergent radiation (Höflich et al. 1996), so the gradient of polarization percentage from red to blue reflects the increasing number of such depolarizing transitions in the blue and ultraviolet portion of the spectrum (Howell et al. 2001). Note that this interpretation does depend on our choice for the ISP, which we will revisit at the end of this section.

The detailed form of the undulations seen in q_{RSP} is therefore a direct probe of the line opacity in the continuum-formation region of SNe Ia, as wavelengths of greater line opacity should show more depolarization. Inspection of plots of the expansion opacity given in Pinto & Eastman (2000) and Kasen (2006) shows a local maximum in the line opacity near 5300 Å and a minimum near 4600 Å, similar to the wavelengths of local minima and maxima, respectively, in the polarization data shown in Figure 4. This correspondence may only be suggestive, but can be verified by modern 3D radiative transfer calculations of the type described by Kasen et al. (2006).

The amplitude of continuum polarization gives information about the global degree of asphericity of the SN atmosphere (Shapiro & Sutherland 1982; Jeffery 1991; Höflich 1991). SN 1999by was the first SN Ia with a firm detection of intrinsic polarization, at least 0.7% (Howell et al. 2001). The best-fit model of Howell et al. (2001) explained the polarization

as being due to an oblate ellipsoid with the major axis 17% longer than the minor axis and viewed nearly equator-on. Despite the sometimes large line polarizations, subsequent observations of SNe Ia have yielded detections of intrinsic continuum polarization that are smaller than in SN 1999by, with values of 0.3–0.4% being typical (Wang et al. 2003, 2006; Leonard et al. 2005; Chornock et al. 2006). Converting the continuum polarization to a geometry is model-dependent (e.g., Höflich 1991), but the lower polarizations of most SNe Ia may be due to objects with asphericities closer to 10% (Wang et al. 2003). SN 2004S is no exception, with a minimum of 0.4% intrinsic continuum polarization.

The polarization angle rotations described above in line features of Si II, Ca II, and Fe II are evidence that the geometric distribution of these ionic species within the ejecta differs from the geometry of the continuum-emitting SN atmosphere. The pure ellipsoidal models of SN 1999by explored by Howell et al. (2001) had only radial variations in composition, but they were able to successfully model the spectropolarimetric feature associated with Si II present in their data. The additional opacity present in the strong line relative to nearby wavelengths resulted in additional depolarization at a constant polarization angle. Such a model for SN 2004S could possibly explain the dip in q_{RSP} seen in our data centered on the Si II line, but not the feature in u_{RSP} . In particular, the loop in the $q - u$ plane for the feature associated with the Ca II NIR triplet cannot be formed in a simple axisymmetric model for the ejecta.

The HV material in SN 2001el also showed such a $q - u$ loop (Wang et al. 2003; Kasen et al. 2003). Kasen et al. (2003) explored several different geometries for the HV ejecta and found that $q - u$ loops were a generic consequence of systems whose components had different axes of symmetry. For example, they found that an ellipsoidal shell whose axis of symmetry was misaligned with respect to an ellipsoidal continuum region produced such a loop. They also found that models invoking clumps in the ejecta could produce $q - u$ loops. Clumps can produce polarimetric signatures by selectively blocking and depolarizing part of the light from the underlying polarized continuum. These clumps might not be oriented along the symmetry axis of the system, and hence produce polarimetric angle rotations.

In SN 2004S, however, the main line-polarization features are being formed at photospheric velocities. This can be seen most clearly in the Si II panels of Figure 6. While modulations of the polarization exist at all wavelengths, the wavelength bins with the greatest polarization deviations from that of the continuum are located just blueward of the P-Cygni absorption minimum. The main source of polarization could be clumps of Si II-absorbing material selectively blocking portions of the polarized photosphere and confined rather narrowly in velocity space above the photospheric velocity. Support for this picture comes from the two separate polarimetric features seen in the Ca II NIR triplet. Explana-

tions for the line polarization must prevent the polarization feature associated with $\lambda 8662$ from blending with the polarization feature formed by $\lambda\lambda 8498, 8542$, just 4000 km s^{-1} to the blue. Depolarizing clumps in the ejecta confined to velocities less than $\sim 13,000 \text{ km s}^{-1}$ could be responsible.

Leonard et al. (2005) described spectropolarimetric angle rotations in line features of Si II and Ca II in SN 2003du that are at least broadly similar to these results. They ascribed the rotations to either clumps in the ejecta or ionization asymmetries of the sort invoked by Chugai (1992) to explain observations of SN 1987A. Clumps of radioactive ^{56}Ni formed in the explosion could produce local variations in ionization and electron density that would be manifested as polarization features. In addition, Wang et al. (2003) describe a potential “skin effect” as ^{56}Ni clumps produce a tangential component to the radiation field whose effects would vary as a function of wavelength due to the wavelength dependence of the photospheric radius. However, any clumps of ^{56}Ni would only have a modest effect on the ionization state of SN Ia ejecta and the significant path length of gamma rays in the ejecta would tend to smooth out the effects of clumpy energy deposition from radioactive elements. Therefore, we do not favor the interpretation where polarimetric effects are directly due to the clumpy distribution of ^{56}Ni instead of the clumpy distribution of those ions directly responsible for the polarimetric features.

Clumps of intermediate-mass elements could be detectable by other means. Thomas et al. (2002) examined the consequences of clumping on variation in line profiles. In their parameterized models, the observed homogeneity of Si II line profiles in SNe Ia meant that the characteristic size scale of perturbations in composition must be of order 1% of the size of photosphere or smaller. Larger perturbations would result in variations of the line profile when observed from different orientations that are larger than the observed variation in normal SNe Ia, though we note that in this particular object the Si II line is somewhat weaker than normal (§3.1; Krisciunas et al. 2007). A single clump in front of the SN photosphere can result in large observed polarizations (Kasen et al. 2003), so perhaps the small value of the polarization modulations in the lines is a result of many small clumps, consistent with the Thomas et al. (2002) results. Future numerical work will make possible quantitative calculations of the effects of clumps of different size scales on the polarization spectrum (Kasen et al. 2006).

Next we turn our attention to the HV lines. The evidence presented above shows that the line-polarization features in SN 2004S are associated with material near the photospheric velocity, not the HV line-forming region. A small polarization modulation is visible in u_{RSP} in the blue wing of the HV Ca II NIR triplet feature. A formal integration over $7875\text{--}8075 \text{ \AA}$ (blueshifts of $17,000\text{--}24,000 \text{ km s}^{-1}$ relative to $\lambda 8542$) gives a non-zero measurement of

$u_{RSP} = 0.103 \pm 0.025\%$, which is significantly smaller than the photospheric feature. Naively, this is somewhat unexpected as SNe 2001el, 2002bf, and 2004dt all showed strong ($0.7\% < P < 2.5\%$) polarization features in their HV features (Wang et al. 2003; Leonard et al. 2005; Wang et al. 2006). The answer may be that we caught SN 2004S at a special epoch, when the HV material had sufficient optical depth (or a large enough photospheric covering fraction) to imprint an absorption feature on the spectrum, but not enough to result in a significant polarization feature.

The time series of spectropolarimetry presented in Wang et al. (2003) showed that the HV polarization feature in SN 2001el was strong at early times and disappeared after maximum light as the feature in the flux spectrum also faded. Our data are most closely comparable in time to their 2001 October 9 epoch (+10 d after maximum light), in which the HV flux feature was still present, but fading, and the polarization feature was mostly gone. SN 2003du provides another example of this phenomenon. Gerardy et al. (2004) presented spectra at early times that showed a strong HV feature, but the data analyzed by Leonard et al. (2005), taken 18 d after maximum light, show no HV absorption or associated polarization feature.

A comparison between the polarimetry of SNe 2001el and 2004S is very interesting. Leonard et al. (2005) found that the spectropolarimetric properties of SNe Ia were diverse, but may be correlated with the photometric and spectroscopic properties. In this case, Krisciunas et al. (2007) demonstrated that these two supernovae have almost identical light curves and spectra, so we would like to know whether the similarities extend to the polarimetry as well. Fortunately, our single set of spectropolarimetry is at almost the same epoch (+9 d) as one of the observations of SN 2001el presented by Wang et al. (2003) (+10 d), though we do not have a corresponding time series of data. Wang et al. (2003) used a different method to determine the ISP (see below) so our results are not directly comparable, but we can make qualitative comparisons to the data presented in their Figures 9, 10, and 11.

The continuum polarization of SN 2001el has a maximum amplitude of 0.3% and it decreases rather sharply by a few tenths of a percent blueward of $\sim 5400 \text{ \AA}$, which is where SN 2004S also shows a change in continuum polarization. At earlier epochs, the Si II $\lambda 6355$ line in SN 2001el shows deviations from axisymmetry in the form of a $q - u$ loop with an amplitude of 0.5%, similar to what we see in our SN 2004S data, though the feature in SN 2001el mostly faded by +10 d to the $\sim 0.1\%$ level. Some difference in the silicon distribution between the two SNe should be expected from the slightly weaker and redder Si II line in the flux spectrum of SN 2004S (Krisciunas et al. 2007).

As noted above, the HV Ca II NIR triplet polarization feature in SN 2001el largely

disappeared between maximum light and +10 d. The photospheric component of the NIR triplet in SN 2001el has a few tenths of a percent polarization at +10 d, although it lacks the two separate features seen in SN 2004S. SN 2001el also shows no obvious sign of the $q-u$ loop at photospheric velocities apparent in the Ca II feature of SN 2004S. A polarization feature (0.2% in each Stokes parameter) in SN 2001el near 4800 Å on day +10 is not mentioned by Wang et al. (2003), but appears to correspond to the features in SN 2004S which we have associated with Fe II. In summary, SN 2001el has slightly less continuum polarization than SN 2004S and weaker line-polarization features at the epoch most comparable to our data, though the Si II line in SN 2001el at earlier epochs is similar to our data for SN 2004S.

The interpretation of the results presented in this paper is affected by uncertainty in the determination of the ISP. Our choice of ISP has been guided by the belief that the intrinsic polarization at wavelengths less than 5000 Å should be minimal, as detailed by Howell et al. (2001). Another plausible method for estimating the ISP is to obtain observations at a very late epoch, when the electron scattering optical depth should be negligible and any measured polarization can be ascribed to ISP. Wang et al. (2003) obtained such observations for SN 2001el and determined a different value for the ISP than was measured from the first method (Kasen et al. 2003), with no obvious way to reconcile the two possibilities. We lack late-time observations of SN 2004S, so we cannot perform this test.

In this work we have chosen the first ISP method due to the simplicity of interpretation and the lack of a compelling argument for another ISP choice, but for the rest of this section we will examine the consequences of relaxing our assumptions. If we do not choose an ISP along the main axis shown by the continuum data points in Figure 3, then the angle of polarization of the continuum will vary with wavelength. One possible alternative ISP would be near the point (q_{RSP}, u_{RSP}) of $(0.0, -0.3)$ in Figure 5, chosen to minimize the polarization angle rotation through the Si II line as well as the magnitude of the polarization at the minimum of the P-Cygni absorption, but this ISP vector creates problems of interpretation as well. No choice for the ISP can eliminate the $q-u$ loop shown by the Ca II NIR triplet. If we know polarization angle rotations must occur across a feature due to one intermediate-mass element, then perhaps we should expect them in others as well. In addition, the total host-galaxy ISP correction would be uncomfortably large given the low host-galaxy reddening.

Potential ISP vectors other than our chosen one necessarily lead to non-zero polarization at wavelengths below 4000 Å, which would be an important result. Implicit in our discussion of the continuum polarization is a construction whereby continuum radiation is polarized by electron scattering and then subsequently depolarized by bound-bound line-transport processes in the outer part of the SN atmosphere. This picture is backed by detailed numerical

simulations of radiation transport in SNe Ia. Paoldrach et al. (1996) analyzed the 1D deflagration model W7 (Nomoto et al. 1984) and found that at maximum light the optical depth to electron scattering was of order unity near a velocity of 5000 km s^{-1} . The apparent “photospheric” velocities measured from the minima of P-Cygni line features are closer to $10,000 \text{ km s}^{-1}$ due the effects of pseudo-continuous opacity from many weak lines of iron-peak elements.

At the later epoch of our SN 2004S observations (+9 d), the surface of optical depth unity to electron scattering should have receded even more deeply into the ejecta. In reality, the competition between polarizing electron scattering and depolarizing lines occurs over an extended range of radii. The predominance of line opacity over Thomson scattering (Pinto & Eastman 2000) means that at wavelengths of high line opacity, the last scattering of photons occurs at larger radii in the ejecta (e.g., Höflich et al. 1998), which limits the opportunity for those photons to be subsequently scattered by electrons and polarized as they exit the SN atmosphere.

These arguments are based on 1D properties of SN Ia simulations. Non-zero polarization at wavelengths of high line opacity could be a sign of clumps of ^{56}Ni mixed out into the ejecta. Such clumps could result in local enhancements of ionization and hence electrons that could produce polarization at larger radii than expected. Significant outward mixing of ^{56}Ni would be an interesting constraint on explosion models and would also have effects on the photometric rise time and overall light-curve shape. Choosing an ISP vector away from the line in Figure 3 also produces a slow rotation of the continuum polarization angle with wavelength that is hard to understand, though Wang et al. (2003) posit a potential “skin effect”. The time dependence of the polarization effects due to these hypothetical ^{56}Ni clumps is unclear, though obviously our single epoch of observations cannot provide any constraints by itself.

5. Conclusions

We have presented a single epoch of high S/N spectropolarimetry of the Type Ia SN 2004S, which had an intrinsic continuum polarization of 0.4%. This observation adds to a growing body of evidence that normal SNe Ia have global asphericities of order 10–20%. The data points from the continuum are consistent with an axisymmetric geometry such as an ellipsoid. Polarization angle modulations across spectral features due to Si II, Ca II, and Fe II are evidence that the distributions of some elements within the supernova ejecta differ from that of the continuum. One natural interpretation of these data is that we are seeing evidence for clumps of newly synthesized elements. These clumps could be a diagnostic of

turbulent burning during the explosion process (e.g., Gamezo et al. 2005). Previous work has shown non-axisymmetric structures in HV material (Kasen et al. 2003), but here the deviations from axisymmetry are present close to the photosphere.

We argued that the clumps in the ejecta are sufficiently narrowly confined in velocity space to prevent the Ca II NIR triplet polarization features from being blended together. This conclusion could be tested with a time series of spectropolarimetric observations of a future SN Ia starting well before maximum light. At early times these clumps might be hidden because the lines are optically thick at higher velocities. As the absorption minima in the flux spectra recede through the ejecta, the clumps could become visible polarimetrically at later times. In particular, the spectroscopic sequence of SN 2004S presented by Krisciunas et al. (2007) shows that at early times the flux minimum of the Ca II NIR triplet line was at higher velocity than the polarimetric features we see at this later epoch. Spectropolarimetric data of the similar SN 2001el before maximum light (Wang et al. 2003) show no features at photospheric velocities in the Ca II NIR triplet (which has a strong HV component), even though photospheric polarimetric features are visible in the Si II $\lambda 6355$ line (which does not).

A time series of spectropolarimetric data would also be useful in understanding the HV material. SN 2004S is the first SN Ia observed polarimetrically with prominent HV features in the total-flux spectrum that lacked counterparts in the polarization. We argued above that this was likely a consequence of the timing of our observations, as the HV polarization features in the similar SN 2001el also disappeared a couple of weeks after maximum light (Wang et al. 2003). The HV material must decrease in optical depth as it expands, so determining the epoch at which its effects disappear in both the total-flux spectrum and the polarization data has the potential to constrain the optical depth or covering fraction of the HV material, key parameters in any model. Alternatively, we could be viewing the HV material from a special orientation, such as along an axis of symmetry.

The deviations from axisymmetry in SN 2004S are responsible for subtle variations in the polarization across the profiles of some spectral lines and would have been unobservable at lower S/N. Spectropolarimetric observations have the potential to be a powerful probe of SN Ia explosion models; however, quantitative conclusions will have to wait for detailed radiative transfer calculations of current 3D explosion models (e.g., Kasen et al. 2006). In addition, interpretation of the continuum observations is hampered by uncertainties in the removal of ISP, even for objects like SN 2004S suffering small extinction. Progress can be made with observations of a larger set of objects, preferably behind minimal dust columns.

We are grateful to R. J. Foley for assistance with the observations and K. Krisciunas for sharing results in advance of publication. We also would like to thank the referee, D.

Kasen, for his close reading of this manuscript. The data presented herein were obtained at the W. M. Keck Observatory, which is operated as a scientific partnership among the California Institute of Technology, the University of California and the National Aeronautics and Space Administration. The Observatory was made possible by the generous financial support of the W. M. Keck Foundation. We wish to recognize and acknowledge the very significant cultural role and reverence that the summit of Mauna Kea has always had within the indigenous Hawaiian community; we are most fortunate to have the opportunity to conduct observations from this mountain. We also would like to thank the expert assistance of the Keck staff in making these observations possible. This research was supported by National Science Foundation grants AST-0307894 and AST-0607485.

REFERENCES

Benetti, S., et al. 2005, *ApJ*, 623, 1011

Berdyugin, A., Snåre, M.-O., & Teerikorpi, P. 1995, *A&A*, 294, 568

Branch, D., Drucker, W., & Jeffery, D. J. 1988, *ApJ*, 330, L117

Branch, D., Livio, M., Yungelson, L. R., Boffi, F. R., & Baron, E. 1995, *PASP*, 107, 1019

Branch, D., et al. 2006, *PASP*, 118, 560

Chornock, R., Filippenko, A. V., Branch, D., Foley, R. J., Jha, S., & Li, W. 2006, *PASP*, 118, 722

Chugai, N. N. 1992, *Soviet Astron. Lett.*, 18, 168

Clemens, D. P., & Tapia, S. 1990, *PASP*, 102, 179

Filippenko, A. V. 1982, *PASP*, 94, 715

Filippenko, A. V. 1997, *ARAA*, 35, 309

Gamezo, V. N., Khokhlov, A. M., & Oran, E. S. 2005, *ApJ*, 623, 337

Gamezo, V. N., Khokhlov, A. M., Oran, E. S., Chtchelkanova, A. Y., & Rosenberg, R. O. 2003, *Science*, 299, 77

Gerardy, C., et al. 2004, *ApJ*, 607, 391

Hatano, K., Branch, D., Fisher, A., Baron, E., & Filippenko, A. V. 1999, *ApJ*, 525, 881

Hillebrandt, W., & Niemeyer, J. C. 2000, ARAA, 38, 191

Höflich, P. 1991, A&A, 246, 481

Höflich, P., Wheeler, J. C., Hines, D. C., & Trammell, S. R. 1996, ApJ, 459, 307

Höflich, P., Wheeler, J. C., & Thielemann, F. K. 1998, ApJ, 495, 617

Howell, D. A., Höflich, P., Wang, L., & Wheeler, J. C. 2001, ApJ, 556, 302

Jeffery, D. J. 1989, ApJS, 71, 951

Jeffery, D. J. 1991, ApJ, 375, 264

Kasen, D. 2006, ApJ, 649, 939

Kasen, D., & Plewa, T. 2005, ApJ, 622, L41

Kasen, D., Thomas, R. C., & Nugent, P. 2006, ApJ, 651, 366

Kasen, D., et al. 2003, ApJ, 593, 788

Khokhlov, A. M. 1991, A&A, 245, 114

Kozma, C., Fransson, C., Hillebrandt, W., Travaglio, C., Sollerman, J., Reinecke, M., Röpke, F. K., & Spyromilio, J. 2005, A&A, 437, 983

Krisciunas, K., et al. 2007, AJ, 133, 58

Leibundgut, B., et al. 1993, AJ, 105, 301

Leonard, D. C., Filippenko, A. V., Ardila, D. R., & Brotherton, M. S. 2001, ApJ, 553, 861

Leonard, D. C., Li, W., Filippenko, A. V., Foley, R. J., & Chornock, R. 2005, AJ, 632, 450

Li, W., et al. 2003, PASP, 115, 453

Livio, M. 2001, in Supernovae and Gamma-ray Bursts: The Greatest Explosions Since the Big Bang, ed. M. Livio, N. Panagia, & K. Sahu (Cambridge: Cambridge Univ. Press), 334

Martin, R., & Biggs, J. 2004, IAU Circ., 8282, 1

Matheson, T., Filippenko, A. V., Ho, L. C., Barth, A. J., & Leonard, D. C. 2000, AJ, 120, 1499

Mathewson, D. S., & Ford, V. L. 1970, MmRAS, 74, 139

Mazzali, P., Benetti, S., Stehle, M., Branch, D., Deng, J., Maeda, K., Nomoto, K., & Hamuy, M. 2005a, MNRAS, 357, 200.

Mazzali, P., et al. 2005b, ApJ, 623, L37

Miller, J. S., Robinson, L. B., & Goodrich, R. W. 1988, in Instrumentation for Ground-Based Astronomy, ed. L. B. Robinson (New York: Springer-Verlag), 157

Misra, K., Kamble, A. P., Bhattacharya, D., & Sagar, R. 2005, MNRAS, 360, 662

Nomoto, K., Thielemann, F. K., & Yokoi, K. 1984, ApJ, 286, 644

Nomoto, K., Uenishi, T., Kobayashi, C., Umeda, H., Ohkubo, T., Hachisu, I., & Kato, M. 2003, in From Twilight to Highlight: The Physics of Supernovae, ed. W. Hillebrandt & B. Leibundgut (Berlin:Springer-Verlag), 115

Oke, J. B., et al. 1995, PASP, 107, 375

Pauldrach, A. W. A., Duschinger, M., Mazzali, P. A., Puls, J., Lennon, M., & Miller, D. L. 1996, A&A, 312, 525

Phillips, M. M. 1993, ApJ, 413, L105

Pinto, P. A., & Eastman, R. G. 2000, ApJ, 530, 757

Reinecke, M., Hillebrandt, W., & Niemeyer, J. C. 2002, A&A, 391, 1167

Schlegel, D. J., Finkbeiner, D. P., & Davis, M. 1998, ApJ, 500, 525

Schmidt, G. D., Elston, R., & Lupie, O. L. 1992, AJ, 104, 1563

Serkowski, K., Mathewson, D. S., & Ford, V. L. 1975, ApJ, 196, 261

Shapiro, P. R., & Sutherland, P. G. 1982, ApJ, 263, 902

Stehle, M., Mazzali, P. A., Benetti, S., & Hillebrandt, W. 2005, MNRAS, 360, 1231

Suntzeff, N., Globus, A., Galli, L., Whiting, A., & Schmidtbreick, L. 2004, IAU Circ., 8283, 1

Theureau, G., et al. 2005, A&A, 430, 373

Thomas, R. C., Kasen, D., Branch, D., & Baron, E. 2002, ApJ, 567, 1037

Trammell, S. R., Dinerstein, H. L., & Goodrich, R. W. 1993, *ApJ*, 402, 249

Tran, H. D. 1995, *ApJ*, 440, 565

Wang, L., Baade, D., Höflich, P., Wheeler, J. C., Kawabata, K., Khokhlov, A., Nomoto, K., & Patat, F. 2006, *ApJ*, 653, 490

Wang, L., Baade, D., & Patat, F. 2007, *Science*, 315, 212

Wang, L., Howell, D. A., Höflich, P., & Wheeler, J. C. 2001, *ApJ*, 550, 1030

Wang, L., et al. 2003, *ApJ*, 591, 1110

Wells, L. A., et al. 1994, *AJ*, 108, 2233

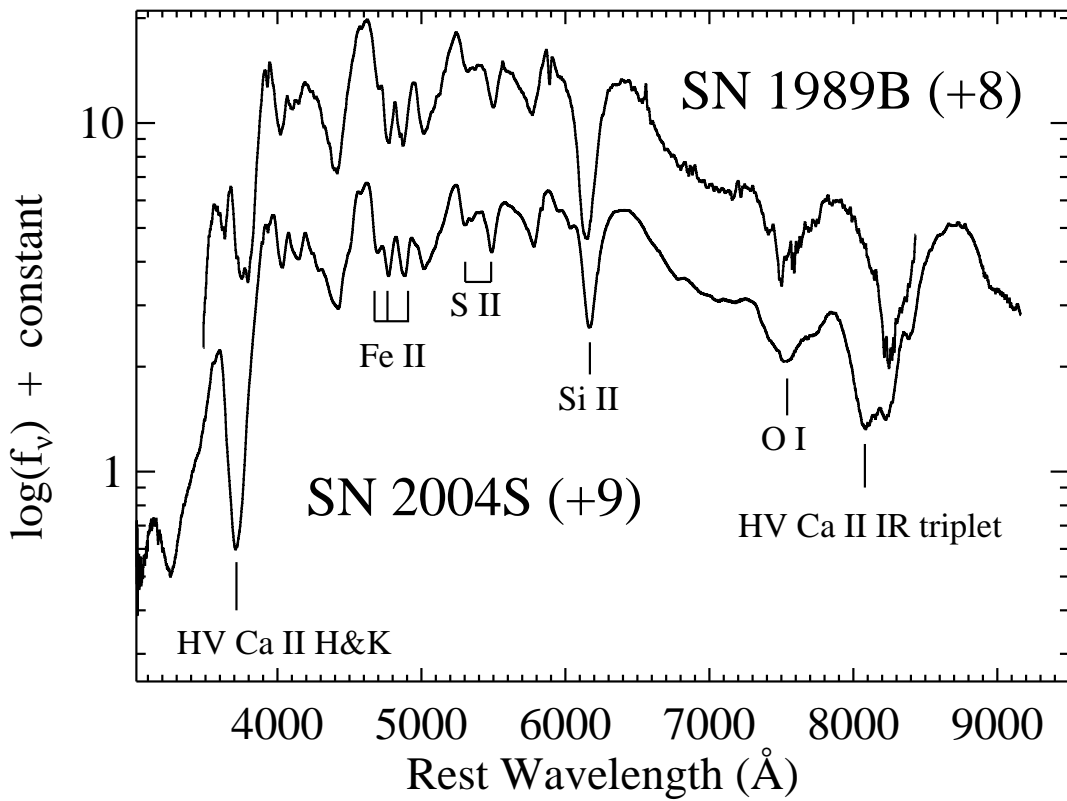


Fig. 1.— Total-flux spectra of SN 2004S and the normal Type Ia SN 1989B from 1989 February 15 (Wells et al. 1994). The numbers in parentheses are ages relative to *B*-band maximum light. Some lines of polarimetric interest are labeled. The major difference between the two spectra is that SN 2004S clearly shows an extra high-velocity (HV) absorption component in both of the spectral features due to Ca II. See Figure 2 for details of these line features. The locations of the members of the Fe II triplet are marked at a blueshifted velocity of 16,000 km s⁻¹.

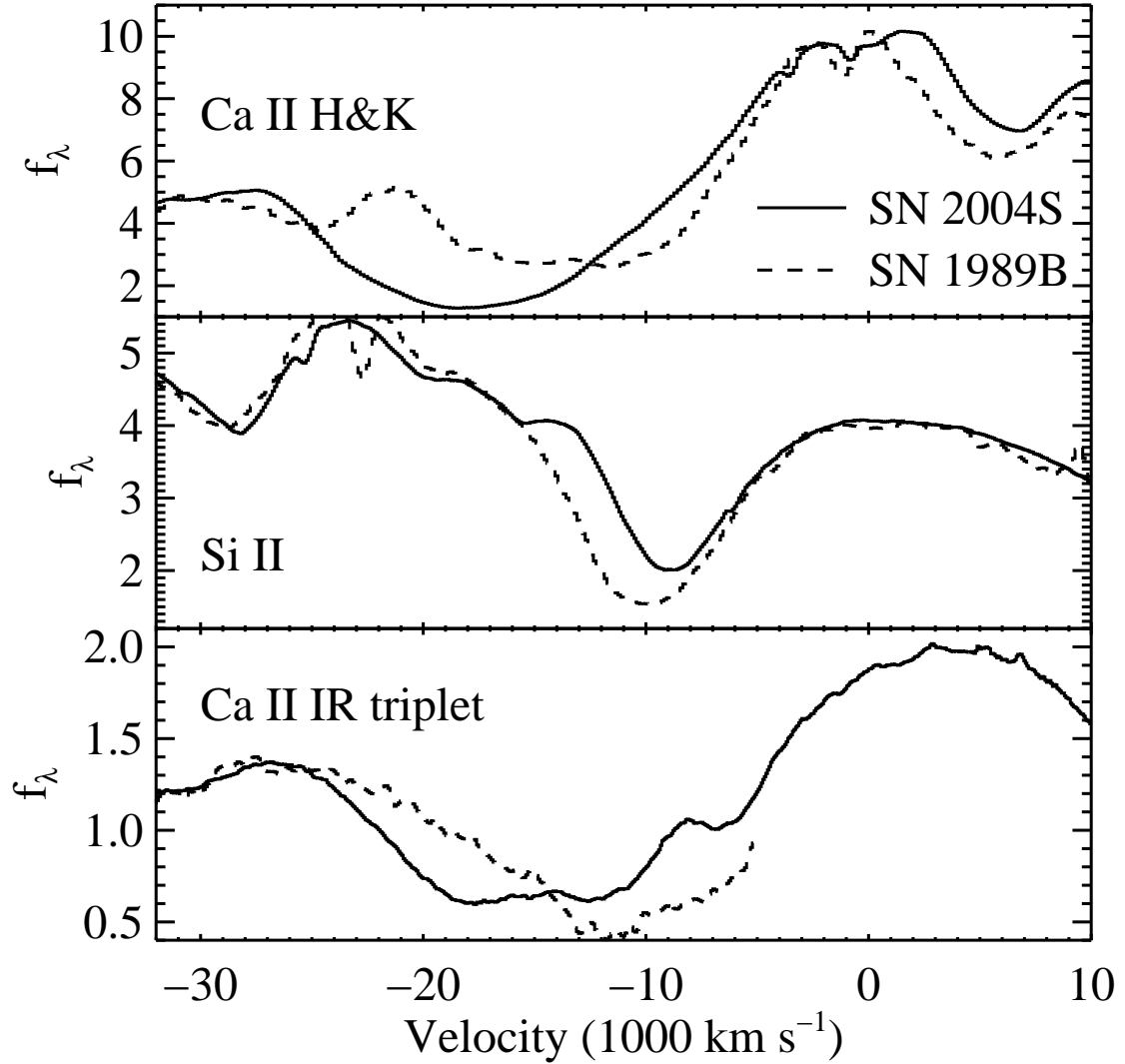


Fig. 2.— Prominent absorption lines in SN 2004S (solid) and SN 1989B (dashed). The velocity axis in each panel is computed relative to the gf -weighted line centroid for each blend (3945 Å, 6355 Å, and 8579 Å, respectively). A separate multiplicative factor has been applied to the flux scale of the spectra in each panel to match the flux peaks of the two objects in order to facilitate comparison of the absorption features. In SN 1989B, all three lines have flux minima at similar velocities (10,000–12,000 km s $^{-1}$), while in SN 2004S an additional absorption component is visible in both of the Ca II features at 18,000 km s $^{-1}$, well above the photospheric velocity defined by the Si II line.

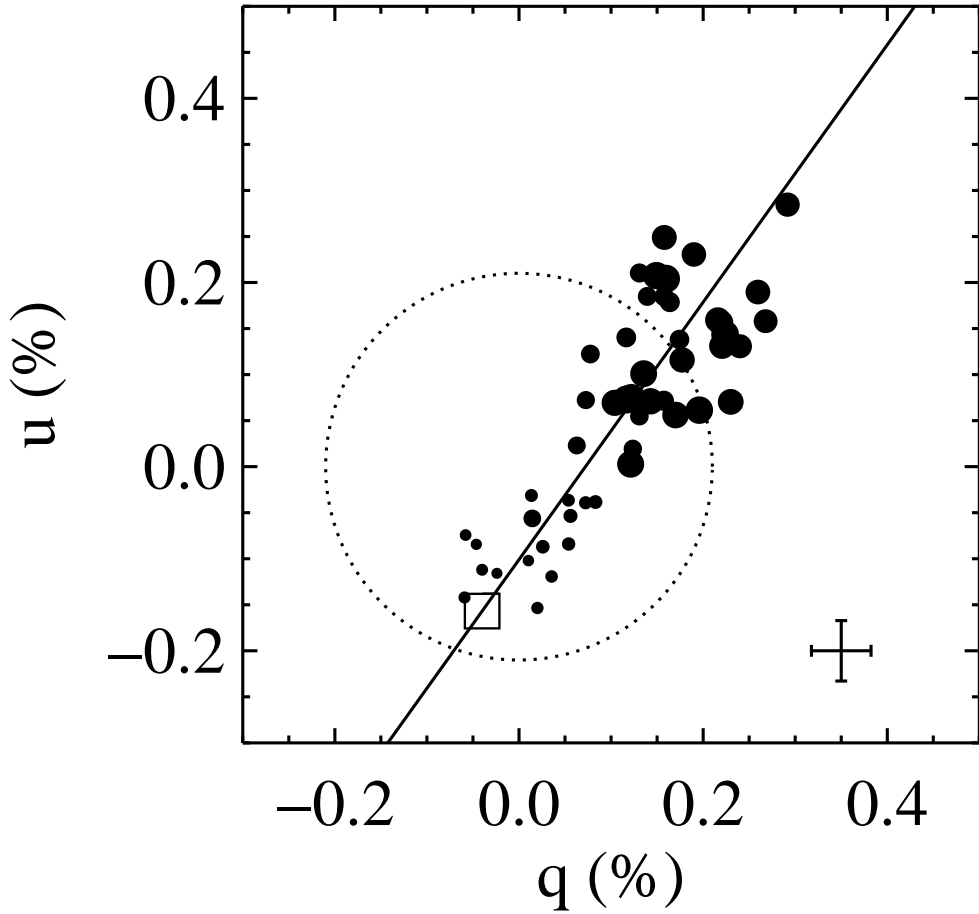


Fig. 3.— Continuum polarization data for SN 2004S in the $q - u$ plane. The data have been corrected for the Galactic component of ISP, as determined from probe stars. Each circle represents a bin of width 50 observed Å selected from wavelength regions free of strong line polarization. See Figure 4 for the definition of these regions. The size of the circles is proportional to wavelength, so a gradient in polarization is evident between the shorter and longer wavelengths. The distribution of points is consistent with a single dominant axis of symmetry for the continuum. The line is a fit to the data points and the box marks a point along the line chosen to represent the host-galaxy contribution to the ISP. The dotted circle has a radius of the maximum expected ISP from host reddening arguments. After subtracting the chosen ISP vector, the data were rotated to align the new Stokes parameter q_{RSP} with the axis of symmetry represented by the line. The cross at $(0.35, -0.2)$ shows the median statistical error bars of the points in the plot.

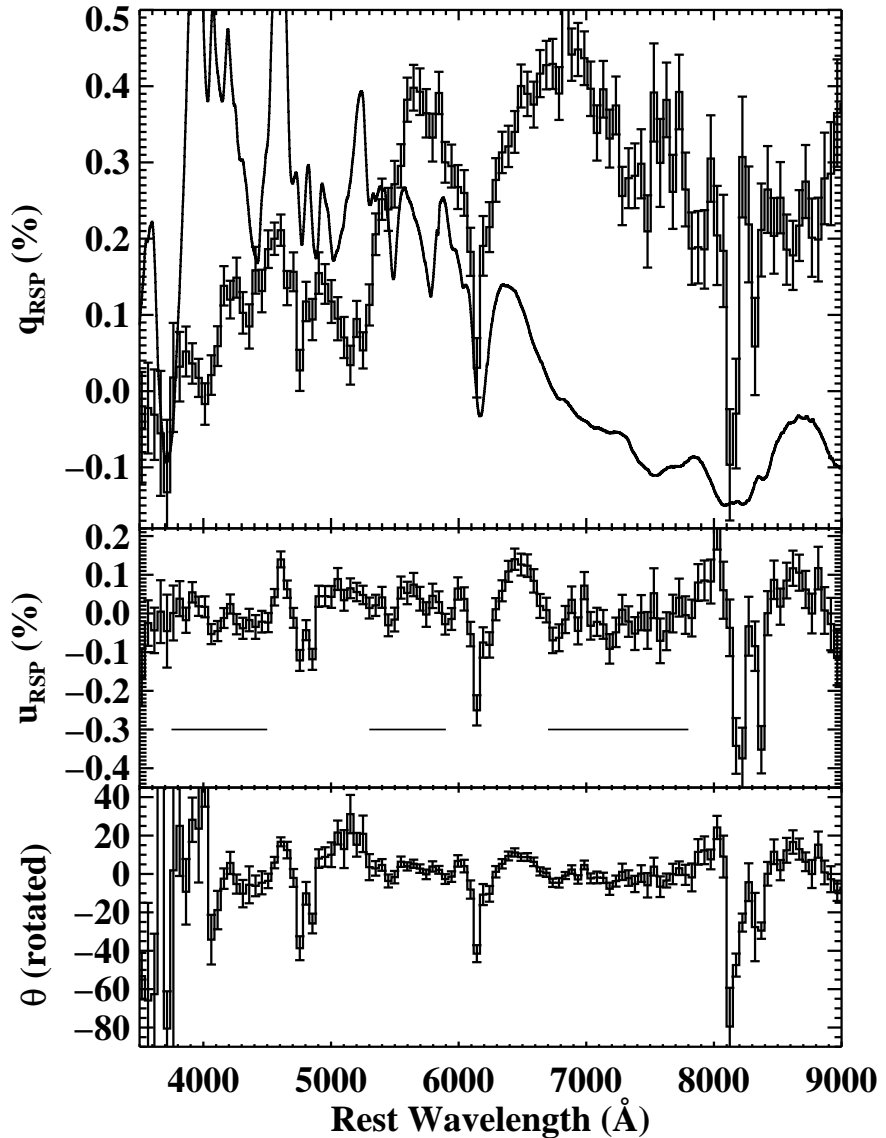


Fig. 4.— Spectropolarimetry of SN 2004S. The polarization data plotted here have been corrected for ISP and binned to 50 observed Å per bin for display purposes. In addition, the Stokes parameters have been rotated to a new coordinate system (q_{RSP} , u_{RSP}), as described in the text. The total-flux spectrum is plotted in the background of the top panel to guide the eye. Rotations due to line features of Fe II, Si II, and Ca II are visible in u_{RSP} and θ . The horizontal lines overplotted in the middle panel represent sections of the spectrum that are free from strong line polarization features and are used to define “continuum” polarization data points in Figures 3 and 5. Note that the angle is ill-defined for wavelengths less than 4200 Å due to the polarization data points being close to the origin of this coordinate system.

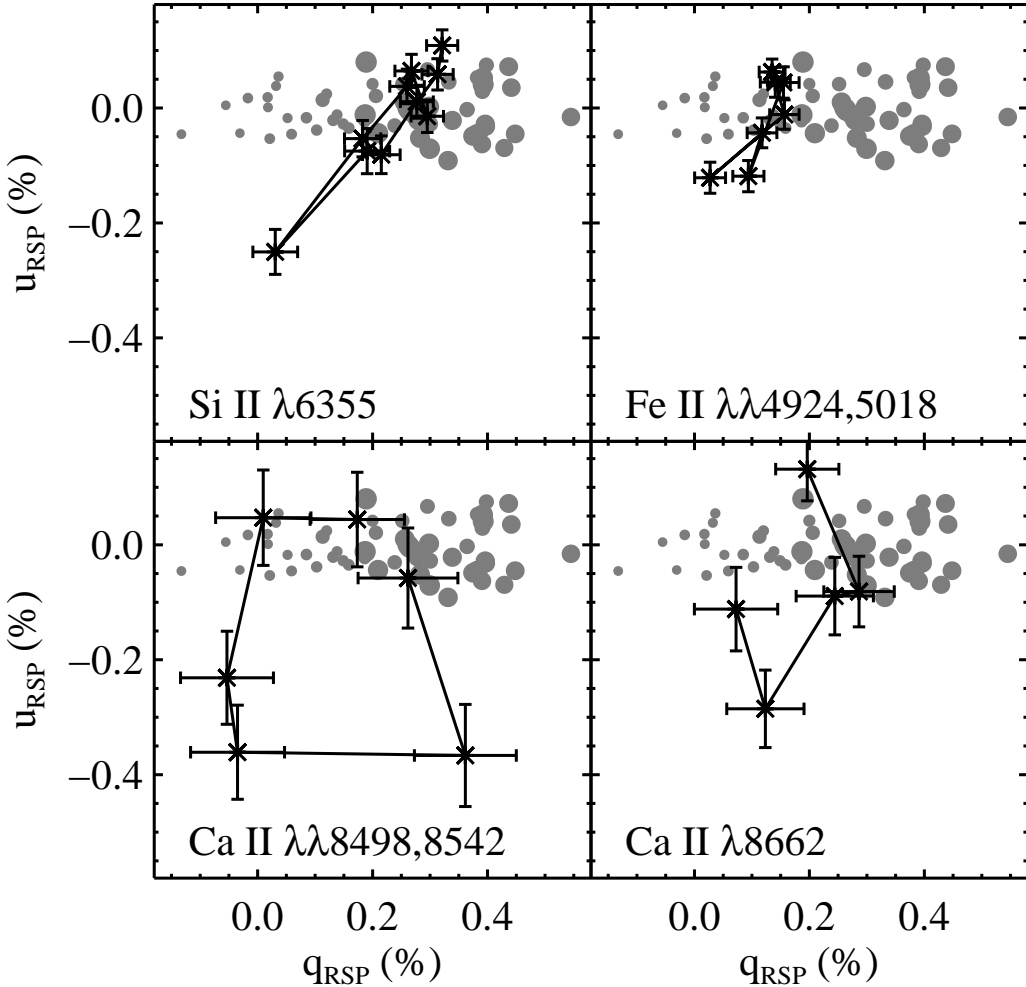


Fig. 5.— Polarization of various spectral features in the $q - u$ plane. The gray circles in the background of each panel represent the same wavelength bins from the continuum windows marked on Figure 4 and shown in Figure 3, but rotated to the new coordinate system. The continuum points are clearly extended along a single line in the $q - u$ plane, indicative of a single axis of symmetry. The points representing wavelength bins associated with spectral features due to each ion (shown in black with error bars) fall outside the spread of continuum points, implying that the lines do not have the same spatial distribution as the continuum. The Si II and Fe II features show similar polarization behavior that may reflect a common spatial origin. The Ca II data points are inconsistent with a simple single-axis symmetry because they show a spread in both q_{RSP} and u_{RSP} . The feature associated with Ca II $\lambda\lambda 8498, 8542$ appears to form a loop in the $q - u$ plane.

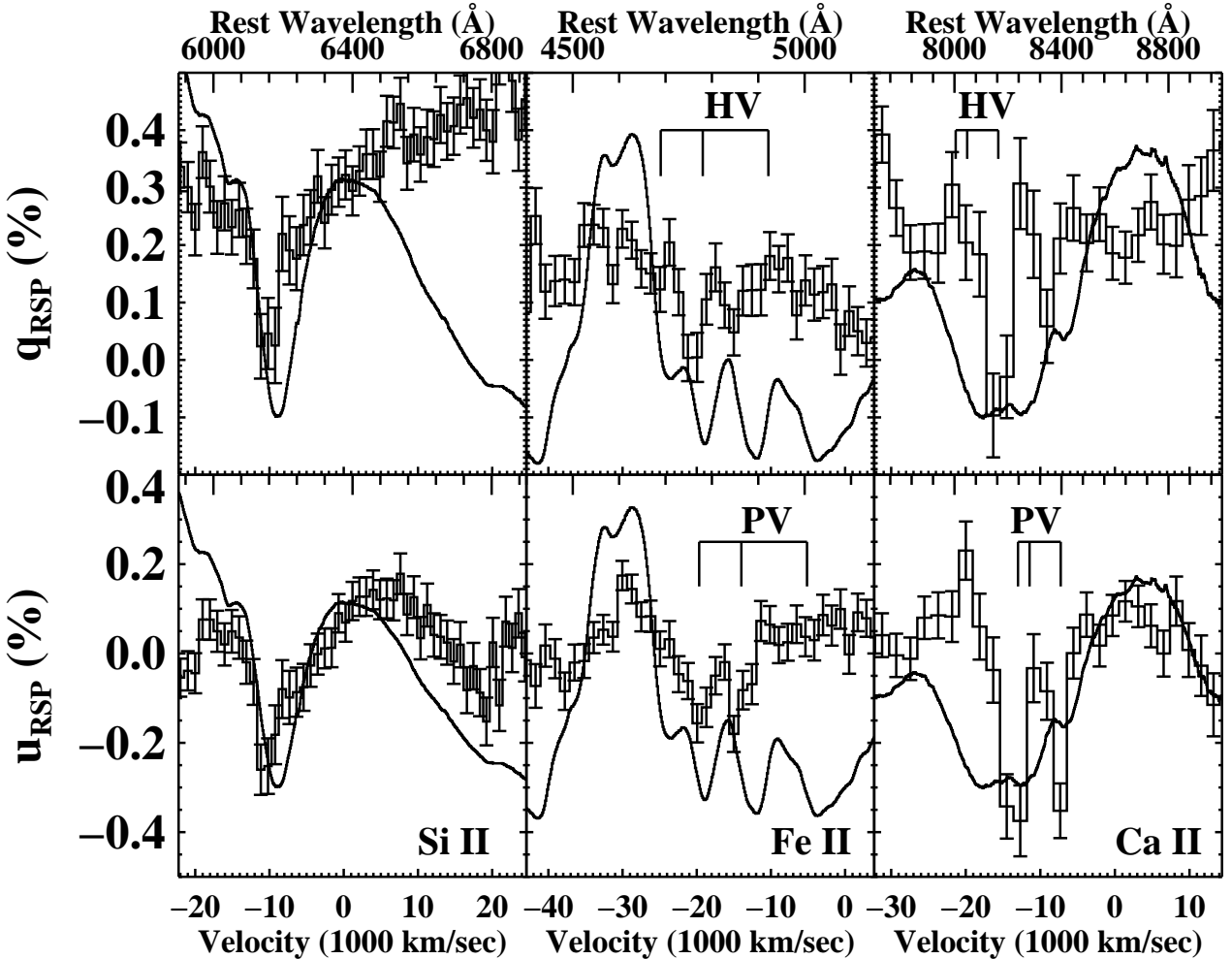


Fig. 6.— Stokes parameters versus velocity for three species. The total-flux spectrum is overplotted in each panel to guide the eye. The line velocities used for the coordinates are relative to the *gf*-weighted line wavelength for each ionic blend. Si II $\lambda 6355$ shows a broad polarization depression with a superposed narrow feature, present in both q_{RSP} and u_{RSP} , and centered at $10,000$ km s $^{-1}$, just blueward of the photosphere. To aid in the identification of spectropolarimetric features, overplotted on the Fe II and Ca II panels are the expected wavelengths of each member of the respective triplets, blueshifted both by the photospheric-velocity (PV) and the high-velocity (HV) line-formation region for each ion. The polarimetric features are clearly associated with the PV for both ions, except for the lack of a feature associated with Fe II $\lambda 5169$. There are no strong polarimetric features associated with the HV line-formation region. See text for details.